Applied Thermal Engineering 236 (2024) 121551

Contents lists available at ScienceDirect

Applied Thermal Engineering

journal homepage: www.elsevier.com/locate/apthermeng

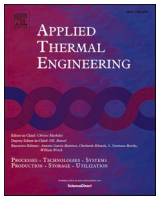

Research Paper

Integration of ocean thermal energy conversion and pumped thermal energy storage: system design, off-design and LCOS evaluation

Alessandra Ghilardi, Andrea Baccioli, Guido Francesco Frate, Marco Volpe, Lorenzo Ferrari *

Department of Energy, Systems, Territory and Constructions Engineering, University of Pisa, Italy

ARTICLE INFO

Keywords:
Ocean Thermal Energy Conversion (OTEC)
Pumped Thermal Energy Storage (PTES)
Energy Storage
Electricity surplus
End-life ship
Round trip efficiency

ABSTRACT

Increasing the penetration of Variable Renewable Energy (VRE) in electric generation systems is a fundamental goal in reducing greenhouse gases emission. To reduce power fluctuations in electricity networks and avoid curtailment, large-scale energy storages represent one of the most promising solutions. Thermally-Integrated Pumped Thermal Energy Storage (TI-PTES) systems are an interesting technology that can be used for this scope if the heat source adopted for thermal integration can provide significant thermal power. The ocean temperature gradient in tropical areas is an attractive heat source to be coupled with the PTES system to realise efficient electric storage when integrated with an Ocean Thermal Energy Conversion (OTEC) system. In this study, a heat pump refrigerated by the warm tropical surface water uses electricity surplus from VRE to heat an amount of water contained in an end-life cargo ship used as water storage. The system discharges the stored energy through an ORC cycle refrigerated by the cold deep seawater when VRE production is low. A preliminary sensitivity analysis of the storage size and temperature is proposed through detailed system modelling to define the optimal design and layout. Therefore, the part-load analysis of the system is assessed to characterise the off-design performances and evaluate the potentialities of this system when applied to a plausible case study that includes VRE generation and an electric demand profile. Finally, the Levelised Cost Of Storage (LCOS) is evaluated and compared to other storage technologies. Results show that the round-trip efficiency may achieve values higher than 60 %, and an equivalent electric battery capacity of 20 MWh is feasible using end-life ships acting as energy storage. In contrast, the obtained LCOS of 388 €/MWh is still not competitive in the energy market. However, since tropical areas have high energy prices, considering this application for remote island electrification could be an interesting solution.

1. Introduction

Moving towards a more sustainable future is nowadays a global priority, and the energy industry is expected to play a primary role in researching new emission-free systems to replace the highly polluting fossil fuel productions. The massive exploitation of Renewable Energy Sources (RES) during the last two decades brought significant savings in pollutant emissions. Consequently, due to the highly variable generation profiles of RES, the electricity networks are facing some operational issues caused by power fluctuations and a non-proper generation/demand matching.

Grid-scale Energy Storage Systems (ESS) are gaining interest as a suitable solution for RES integration, thanks to their capability on load shifting [1]. Among this category, Pumped Hydro Energy Storage (PHES) has traditionally been the most used technology thanks to its high round-trip efficiency (65–85%), long operative life of up to 40 years, and affordability [2]. However, the strong dependence on the geographical site makes PHES less attractive because of its low flexibility. To overcome this issue, grid-scale electro-chemical storage, such as Lithium-ion (Li-ion), Sodium sulphur (NaS) and Redox Flow Batteries (RFB), are suitable alternatives to PHES [3]. Li-ion batteries are one of the most mature ESS because of their high energy efficiency (up to 90–97%) and low maintenance needs. NaS batteries have a high round trip efficiency of around 85% and high energy density as well. They also have lower costs than Li-ion because of their cheaper materials, which can also be recycled (differently from Lithium ions). However, operational costs [1]. RFB, instead, work at ambient temperature maintaining a high round trip efficiency of up to 85%, but their competitiveness is limited due to high operating costs and low energy density [4]. To

* Corresponding author ate: Department of Energy, Systems, Territory and Constructions Engineering, University of Pisa, Largo Lucio Lazzarino, Pisa 56122, Italy.
E-mail addresses: alessandra.ghilardi@phd.unipi.it (A. Ghilardi), andrea.baccioli@unipi.it (A. Baccioli), guido.frate@unipi.it (G.F. Frate), m.volpe2@studenti.unipi.it (M. Volpe), lorenzo.ferrari@unipi.it (L. Ferrari).

https://doi.org/10.1016/j.applthermaleng.2023.121551
Received 3 February 2023; Received in revised form 4 August 2023; Accepted 6 September 2023
Available online 7 September 2023

Nomenclature

Acronyms

CAES	Compressed Air Energy Storage
CAPEX	Capital Expenditure
CB	Carnot Battery
CEPCI	Chemical Engineering Plant Cost Index
COP	Coefficient Of Performance (-)
CRF	Capital Recovery Factor
ESS	Energy Storage System
RFB	Redox Flow Battery
HE	Heat Engine
HP	Heat Pump
Li-ion	Lithium-ion
LAES	Liquid Air Energy Storage
LCOS	Levelised Cost of Storage
LT	Low Temperature
HT	High Temperature
NaS	Sodium Sulphur
ORC	Organic Rankine Cycle
OPEX	Operational Expenditure
OTEC	Ocean Thermal Energy Conversion
PHES	Pumped Hydro Energy Storage
PTES	Pumped Thermal Energy Storage
PV	Photo Voltaic
RES	Renewable Energy Sources
ST	Storage Tank
TI-PTES	Thermally Integrated Pumped Thermal Energy Storage
VRE	Variable Renewables Energy

Subscripts

c	Cold
ch	Charge
d	design
dis	Discharge
D	Darcy
e	External
i	Internal
N	Operating life in years
off	Off-design
r	Re-injection
rt	Round-trip
s	Storage
surf	Surface
w	Water

Symbols

A	Area (m^2)
c_P	Specific heat (J/kgK)
D	Diameter (m)
E	Energy (Wh)
f	Darcy's friction factor (-)
h	Heat transfer coefficient (W/m^2K)
Nu	Nusselt number (-)
η	Efficiency (-)
ρ	Density (kg/m^3)
L	Length (m)
k	Thermal conductivity (W/mK)
v	Velocity (m/s)
$\dot{m}$	Mass flow rate (kg/s)
$\dot{W}$	Mechanical power (W)
P	Pressure (Pa)
Pr	Pradtl number (-)
R	Discount rate (-)
Re	Reynolds number (-)
T	Temperature (°C)
U	Global heat transfer coefficient (W/m^2K)
Δ	Difference
τ	Constant time (h)

overcome these limitations, Carnot Batteries (CB), which include Liquified Air Energy Storage (LAES) and Pumped Thermal Energy Storage (PTES), are suitable alternatives [5]. CBs can store electric energy as thermal energy and convert it back to electricity using commercially available components, such as compressors, pumps, turbines, and heat exchangers, making them easily scalable, manageable and site independent. LAES systems overcome geographical limitations because the liquid air is stored at atmospheric pressure in liquid form (with reduced storage volumes) and have a long operational life (30–40 years) as well, but round-trip efficiency does not exceed 50–60% due to the complexity of the liquefaction system [6]. PTES systems are similar to LAES because of their high energy density, site independence, and lifetime (25–30 years). In addition, PTES have a lower plant complexity which brings to higher round-trip efficiencies (70–80%) and lower maintenance costs. For these reasons, PTES is considered one of the most promising grid-scale ESS to support VRE integration.

PTES systems store electric energy as thermal exergy in artificially built tanks through different charging technologies, such as Heat Pumps (HP) or electric resistors, able to transfer heat from a Low Temperature (LT) reservoir to a High Temperature (HT) reservoir [7]. The discharging phase converts the stored thermal energy into electric energy through a Heat Engine (HE), typically a Brayton or an Organic Rankine Cycle (ORC). Starting from the standard layout that includes an HP, two thermal reservoirs and a HE, PTES can assume different configurations, depending on the discharging cycle. Brayton-based PTES uses an HE for the discharging phase, with argon, helium or air as working fluid, with round-trip efficiency ranging from 50 to 75% [8]. Concerning the storage medium, packed beds with rocks are proposed in [9] for working temperatures up to 1000 °C, while liquid tanks are used in [10] for temperatures up to 500 °C. The alternative configuration, the Rankine PTES, uses a Rankine cycle for the discharge. They usually operate at lower temperatures, in the range of 100 °C and 250 °C, using sensible storage media, which is usually pressurised water, latent, or both [11]. Since operating temperatures are low, organic refrigerants, ammonia, or water are the most common working fluids for subcritical applications. Round-trip efficiencies are in the range of 50–60%, which is lower compared to the Brayton layout. However, working with lower temperatures brings easier management, and the number of heat exchangers can be reduced using reversible configuration, thus lowering the capital costs compared to the Brayton configuration [12].

The poor performance of a Rankine PTES can improve by providing some thermal integration [131415]. Thermal integrated PTES (TI-PTES) exploit an external heat source to enhance the round-trip efficiency by delivering heat at a temperature higher than the ambient, returning a round-trip efficiency higher than 100% [16]. The benefit of thermal integration is significantly high when the temperature level of the additional heat source is close to the storage temperature. For this reason, it is not worth using heat provided by fossil fuel combustion, while low grade heat exploitation is interesting. In literature, different thermal sources are proposed as a thermal integration, including district heating network, solar radiation (through solar collectors) [17], geothermal reinjected brine and waste heat sources [18].

However, an alternative thermal source for integration can be the ocean thermal gradient naturally provided by solar radiation in tropical

regions. To the authors knowledge, this thermal integration was never investigated in the literature. The ocean temperature gradient, indeed, translates into an exploitable ΔT to be coupled into a TI-PTES. Despite this thermal integration is exploitable only in suitable regions (i.e., remote islands in tropical zone), it could be beneficial to decarbonise those regions by integrating VRE coupled to a storage capacity (the TI-PTES). In these areas, a nearly constant temperature difference ΔT of around 20 – 25 °C exists between the warm surface seawater and the depth cold seawater. Traditionally, ocean thermal potential exploitation for energy purposes has already been proposed since the early 1900 s thanks to Ocean Thermal Energy Conversion (OTEC) systems [19]. OTEC systems can produce electric energy by taking advantage of the temperature difference Δ T between warm surface seawater (26–28 °C) used for the working fluid evaporation and deep cold seawater used for the condensation phase through a direct Heat Engine (HE). Geographical regions characterised by a suitable and exploitable Δ T are usually located near tropical latitudes. The surface water temperature is nearly constant over the year, and the bathymetry is adequate [2021]. Several OTEC configurations have been proposed in the literature, including mainly open-cycle plants and closed-cycle plants. Open loop configuration uses seawater directly as the working fluid [22]. Despite the fact that they have a lower capital cost compared to the closed loop configuration, larger turbines are necessary due to the larger specific volume of the seawater. For these reasons, the most recent OTEC configurations proposed in the literature are based on the closed-loop cycle [23]. Closed-loop cycles have the advantage of choosing the desired working fluid, thus limiting the dimension of the components. However, large exchanging areas are required, determining the heat exchangers to be constructed with materials resistant to the highly corrosive environment (the seawater), which determines a higher investment cost [24]. OTEC plants have been proposed both in the on-shore configuration and on the off-shore one, which includes the necessity of having a floating platform as a side infrastructure. Furthermore, OTEC systems require some additional facilities, mainly represented by the pipeline, to pump up the cold water from the seabed at 800 – 1000 m depth, which means a significant pumping duty. Additional issues related to biofouling can then show up, thus requiring other maintenance [25]. Due to the limited temperature level of the HT reservoir, OTEC plants use an Organic Rankine Cycle (ORC) to produce electricity from low-enthalpy hot sources [26]. Although a low efficiency of around 3% characterises OTEC plants due to the limited available Δ T, they represent a promising technology for decarbonisation purposes. Even though they are constrained to the geographical location, then, decarbonisation can be particularly impacting if applied to tropical regions, in which fossil fuel-based generation systems are still massively used. As a conclusive remark of this section, it is worth noting that OTEC plants have been investigated as a stand-alone technology to provide electricity to remote islands and thus avoid using fossil fuels. Despite that, their low efficiency and the operational challenges still pose some limitations on OTEC applicability to integrated systems.

However, the OTEC operational flexibility in grid-scale contexts that include VRE generation, could be enhanced by integrating it with a storage capacity. Literature provides a few study about OTEC integration with VRE, such as wind turbines [27] and PhotoVoltaic modules [28]. In the latter reference, an hydrogen storage capacity is also integrated into the system, showing that it brings benefits to the overall energy efficiency. However, integrating OTEC with a storage capacity remains still barely investigated. The coupling of PTES with OTEC systems, then, could be an interesting solution both aiming to increase the efficiency of a PTES system with ocean thermal integration and to enhance the flexibility of systems that require to manage variable generation from RES and variable electric demand. Nowadays, both the OTEC and the PTES systems are known as stand-alone technologies, thanks to the scientific papers cited in the literature review and a few pilot plants. However, systems that include the two of them never be investigated.

In this paper, the authors propose then the integration of an OTEC plant acting as the discharge phase of a TI-PTES storage capacity. In this framework, the OTEC can act as “renewable integration” to the PTES system and as a stand-alone generation unit when the storage charge/discharge is not required. By doing so, the integration of VRE is then supported by the PTES storage capacity, which provides additional flexibility and load-shifting capabilities. Therefore, this paper proposes the analysis of the performance of a thermo-electric storage PTES thermally integrated by an OTEC system to examine its benefits in terms of operational flexibility. Different plant layouts will be studied, optimising the round trip efficiency of the storage system as the storage temperature varies using Aspen Hysys software for numerical simulations. In addition, the massive amount of thermal energy contained in the oceans and the possibility of using end-life cargo ships as thermal storage would allow the construction of high-power Carnot batteries directly operating on national grid storage to reduce fluctuations caused by VRE and confer the system flexibility.

1.1. Objectives and contribution

The study aims to investigate a Rankine TI-PTES system using the thermal ocean temperature gradient as thermal integration, considering the discharging phase is realised by an OTEC system. The analysis of the system is carried out through three main objectives, structured as follows:

- Optimal design through round-trip efficiency optimisation. This first part of the analysis aims to identify the most performing plant configuration via maximising the round-trip efficiency. By doing so, the optimal storage temperature is found, so the size of the components, especially the storage volume;
- Once the optimal plant layout and size of the components are found, a part-load analysis is carried out to characterise the off-design performances when the plant works in non-nominal conditions
- Finally, the proposed TI-PTES system is applied to a realistic case study that includes variable ERS generation and electric demand profiles. This section brings to the technology LCOS evaluation and a comparison with other common ESS in terms of LCOS and round-trip efficiency.

2. Case study

2.1. Case study location and data

The proposed system, as already mentioned, is suitable for tropical regions thanks to their geographical morphology. The San Blas archipelago in Panama (9°34′N, 78°49′O) was selected as a suitable location [29] since it has proper bathymetry and surface seawater temperature profile, as shown in Fig. 1. Data surface water temperature profile and bathymetry are based on [30]. The plant location is supposed to be offshore due to the large storage tank size.

2.2. System architecture and size

Following the Rankine TI-PTES configuration, the system works between three thermal reservoirs, i.e. the Storage Tank (TS) at the temperature T_s, the surface seawater at the ambient temperature T_{amb} and the deep cold seawater at the temperature $T_{c,}$ as shown in Fig. 2. The system architecture is composed of three main sub-systems, summarised as follows:

- A charging cycle operated by a vapour compression HP using surface water at temperature T_{surf} as the cold source and the storage tank at the temperature T_s as the hot source. During the charging phase, thermal energy is stored in the TS at the temperature T_s, which is higher than T_{surf} thanks to the vapour compression HP that uses the

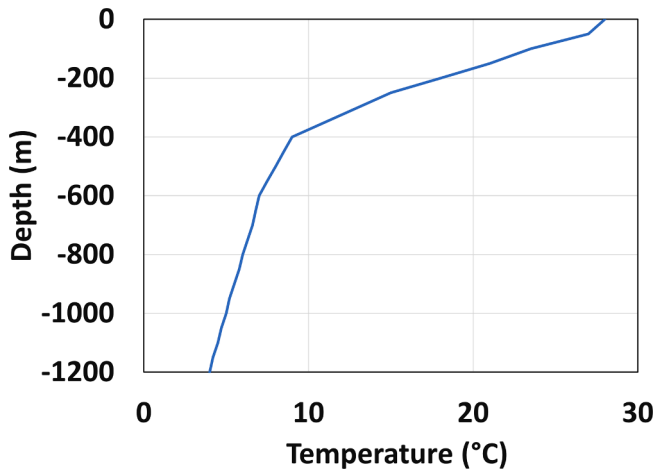

Fig. 1. OTEC selected site bathymetry and.

surface water as the cold source and surplus electric energy from the grid.

- A storage tank (ST) where a fluid is stored at $T_s > T_{surf}$. The HP working fluid releases a heat flow rate during the condensation phase warming up the storage fluid. Once the storage is charged, it is ready for the discharging phase operated by the OTEC system when it is required according to the electricity demand.
- A discharging cycle made of an ORC, using the TS at the temperature T_s as the hot source for evaporation and the deep seawater at the temperature T_c as the cold source for condensation. The free contribution to the ORC condensation phase is given by sun radiation. The warm fluid inside the storage tank is used to vaporise the ORC working fluid, which drives an expander and is later condensed using the cold deep seawater at the temperature of T_c. A schematic representation of the process is shown in Fig. 2.

A 10 MW nominal power OTEC cycle is selected as the discharge cycle. The nominal discharging duration is set to 2 h for every investigated configuration, while the nominal charging duration is 8 h. The operational parameters for the charging and the discharging phases are summarised in Table 1.

2.3. Working fluid selection

OTEC plants working with the closed loop configuration are usually based on a ORC. The fluid selection broadly influences several system aspects, such as the thermodynamic cycle, the first law efficiency, the components cost (especially the turbine and heat exchangers), the heat transfer process, the plant configuration, safety issues, and environmental restrictions. The authors identified in [29] a shortlist of suitable working fluids for ORCs that satisfy the cited requirements. Despite that, commercial availability, moderate price, non-flammability, and non-toxicity are additional parameters required for this application. In addition, the selected fluid must have a suitable critical temperature value, acceptable condensation temperature [31], and high latent heat to restrict mass flow rates since the cycle works with slight temperature differences during heat exchange processes. Furthermore, the OTEC fluid selection is also based on achieving high thermodynamic and electric efficiency [30]. Considering these restrictions, ammonia is one of the most suitable working fluids considering its appropriate latent heat, heat transfer coefficient, and optimum behaviour in maximising the first law efficiency. Considering the same thermodynamic and environmental performances, ammonia is also selected for the HP charging cycle.

2.4. Storage system

Storages connected to PTES systems dispose of conveniently designed tanks for their application. Phase Changing Materials (PCM) have been commonly hypothesised for Rankine PTES for their compactness (for further details, see [16]). However, PCM-based storages present significative heat transfer issues that force the design of

Table 1
OTEC nominal operating conditions.

	Power (MW)	Duration (h)
Charging phase	Variable with T_s	8
Discharging phase	10	2

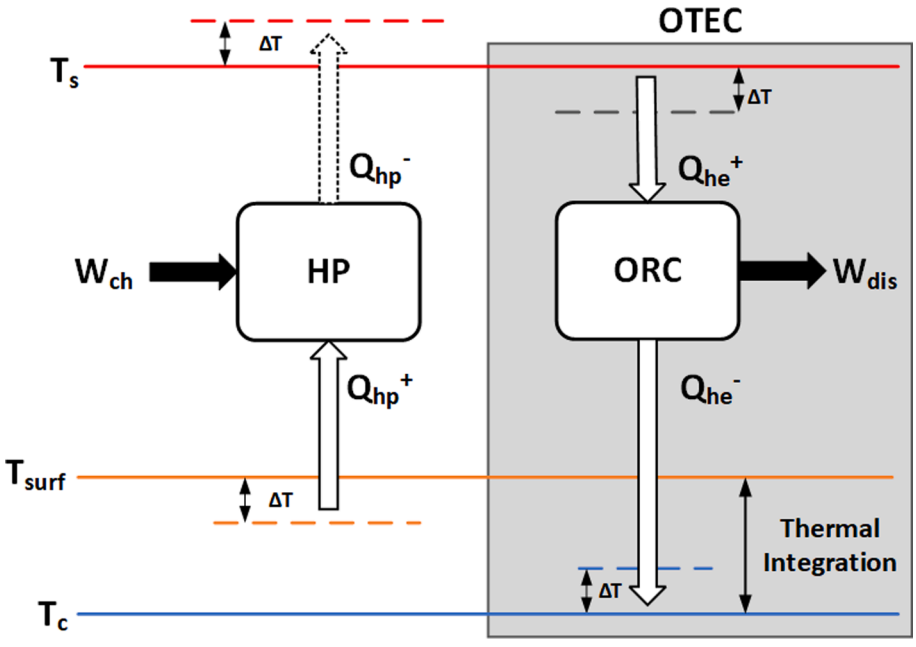

Fig. 2. Conceptual integration of OTEC as the discharging system for the PTES.

heat exchangers to be non-conventional and thus more expansive. This phenomenon is more evident the higher is the system size. In this case, indeed, a grid-scale size is selected for its suitability on the application scenario and also because small-scale OTEC systems are uneconomic due to low efficiency and high components cost. Sensible storage is then examined for this application. In this framework, a sensible water storage is a suitable alternative, given its cheapness and high density as well. Seawater is then used as the storage material because of its availability and accessibility by considering the hypothetic OTEC location. Due to the selected scale size of the plant, the storage tank is supposed to be large. Hypothesising, then, an off-shore application, the plant already needs a floating platform to host the components. For this case study, then, the storage capacity is supposed to be ensured by using a commercial bulk carrier or tanker ship as an end-life ship acting as energy storage. This solution can be interesting to give a second life to cargo ships that otherwise would be scrapped and, at the same time, to provide an already set up infrastructure for the entire plant. The storage volume is supposed to be held in the cargo hold, while the HP and the OTEC are on the top.

2.5. Plant layouts

Different system layouts are proposed and analysed for a broad exploration of coupling OTEC and PTES systems, according to the following terminology:

- ORC with ocean re-injection
- ORC without ocean re-injection
- Recuperated ORC without ocean re-injection

2.5.1. ORC with ocean re-injection

In this configuration, the HP warms up the surface seawater from T_{amb} up to T_s thanks to the electric energy supplied to the compressor. The discharging phase is realised by a Rankine cycle. Ammonia is evaporated by the warm water stored in the tank. The water after the evaporator is directly re-injected into the ocean. In this configuration, the HP realises the entire ΔT from T_{amb} to T_s in the following charging phase. The reference scheme is shown in Fig. 3.

2.5.2. ORC without ocean re-injection

The reduction of the HP compressor power is useful for increasing the COP, consequently, the whole system performance. For this reason, an alternative configuration is proposed. The discharging phase is still realised by a Rankine cycle with ammonia. After the ammonia vaporisation, the cooled hot water coming from the tank is re-circulated and re-injected into the storage tank at a temperature $T_r < T_{amb}$ and not into the ocean. In this way, the HP compression power is reduced for the following charging phase. A reference scheme is shown in Fig. 4.

2.5.3. Recuperated ORC without ocean re-injection

An increase in the discharging cycle efficiency also enhances the whole system performance [13] and decreases the storage size. Therefore, a recuperated ORC is investigated as an alternative configuration to the previous ones to exploit the system potentialities better. A recuperated ORC with ammonia cannot have an internal heat exchanger as traditional ORC systems operate with dry fluids since ammonia is a wet fluid. For this reason, an ammonia spill from the turbine is required, as done in traditional steam cycles. After the ammonia is vaporised, a first expansion is realised in the high-pressure turbine stage, where a certain amount of steam is spilled to recover the liquid ammonia after the circulation pump. The remaining expansion enthalpy gap is realised in the low-pressure turbine stage by the remaining ammonia mass flow rate. The cooled hot water coming from the tank is re-injected into the storage, like in the previously described configuration. A reference scheme is provided in Fig. 5.

2.6. Simulation in a realistic scenario

The preliminary thermodynamics analysis aims to assess the optimal

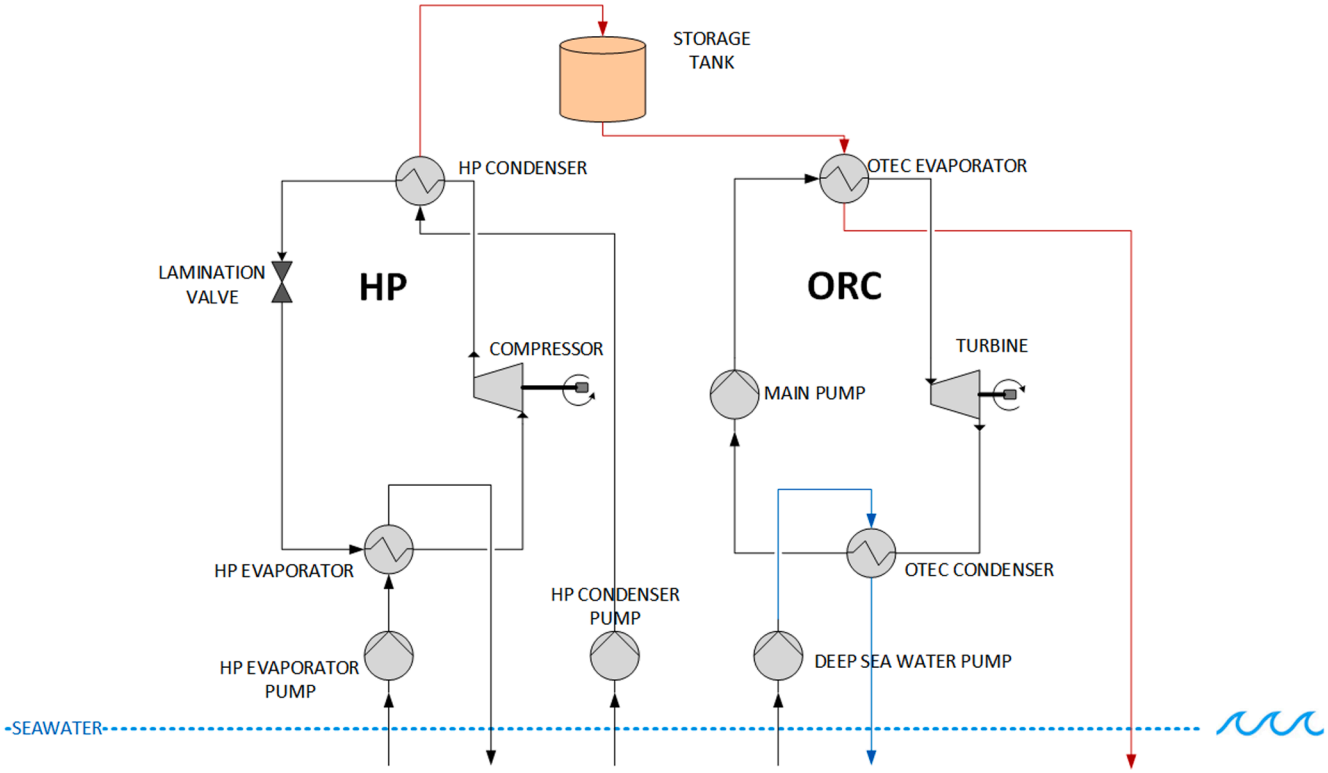

Fig. 3. Simple ORC with ocean re-injection.

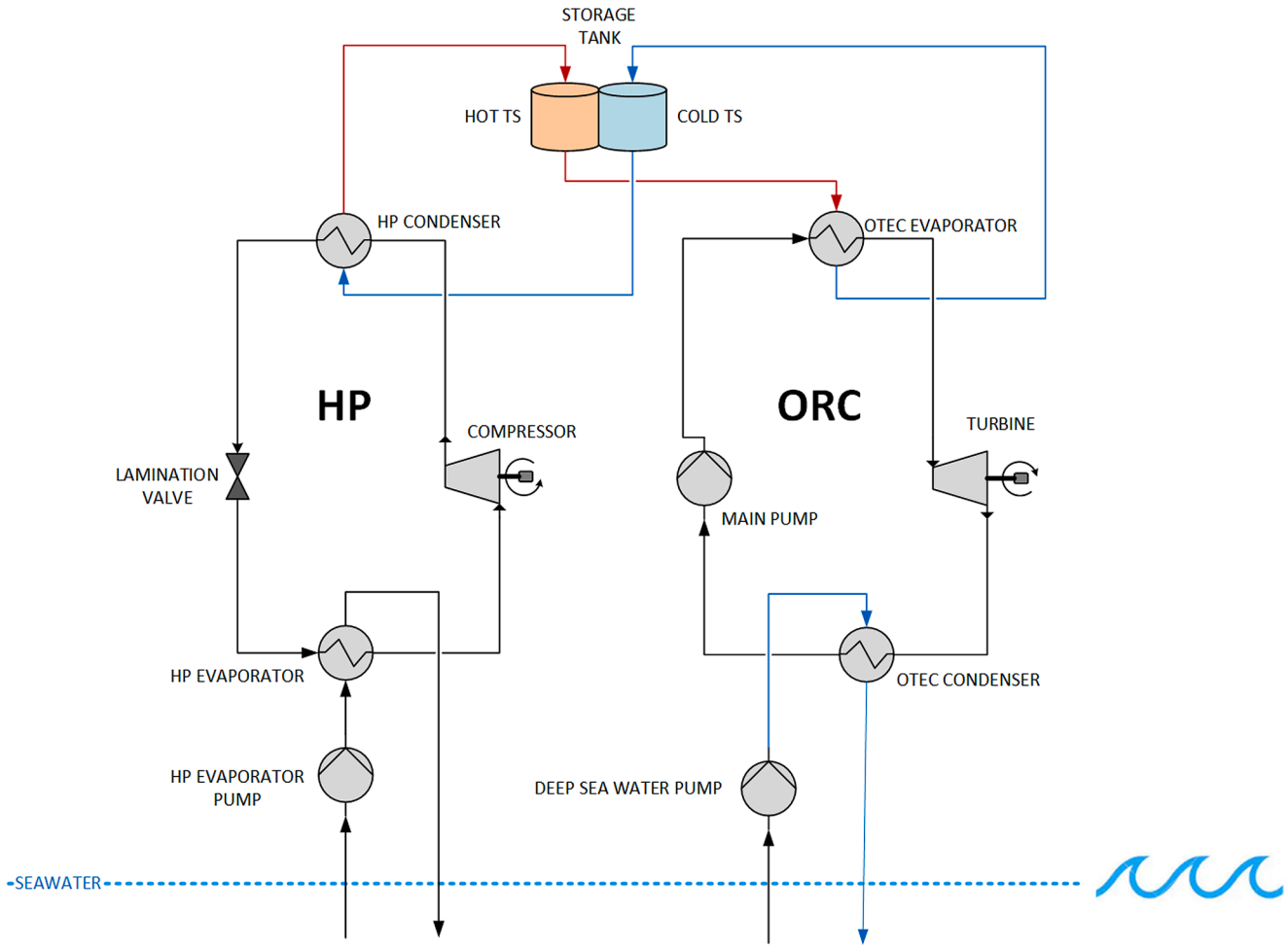

Fig. 4. Simple ORC without ocean re-injection.

design and size of the charging and discharging cycles. After that, the best configuration regarding round trip efficiency and TS volume feasibility is selected to evaluate the Levelised Cost of Storage (LCOS) when the system is used to match the generation and demand profiles of a realistic scenario. Since the integrated PTES-OTEC system proposed in this paper is attractive for decarbonising areas (like the tropical ones), the proposed case study is applied in a context with a high penetration of renewables. The PTES-OTEC system is then able to supply the demand side necessities mainly via three operative modalities represented in Fig. 6:

- Directly through RES production;
- Discharging the TES previously charged by RES surplus;
- Using the traditional OTEC configuration (without using the HP) when the TES is not charged enough;

As a case study, the generation and demand profiles of a plausible scenario are from [32] and scaled on the plant size. Fig. 7 represents the demand and generation profiles for the selected case study, which includes a wind farm of 44 MW and a Photo Voltaic (PV) plant of 7,3 MW.

3. Methodology

3.1. Performance indicators

The key performance indicators for a storage system are round-trip efficiency, which defines its capability to convert back the stored energy, and storage volume, indicating the storage system size and the consequent feasibility [13]. More specifically, the round-trip efficiency represents the ratio between the output electric energy from the discharging phase and the input electric energy given to the charging cycle. In this case study, the round-trip efficiency η_{rt} is the ratio between the net electric output from the OTEC cycle E_{dis} and the electric power of the HP cycle E_{ch}, as shown in Equation (1).

$$\eta_{rt} = \frac{E_{dis}}{E_{ch}} \tag{1}$$

The energy from the discharging phase is calculated as shown in Equation (2), as the integral of the net electric output $\dot{W}_{dis}$ over the discharging time τ_{dis}. The charging electric energy follows the same structure and is given by integrating the compressor electric power needed for the charging phase $\dot{W}_{ch}$ over the time τ_{ch} (Equation (3).

$$E_{dis} = \int_0^{\tau_{dis}} \dot{W}_{dis}(t) \bullet dt(Wh) \tag{2}$$

$$E_{ch} = \int_0^{\tau_{ch}} \dot{W}_{ch}(t) \bullet dt(Wh) \tag{3}$$

The net electric power coming from the OTEC discharging cycle includes the electric power generated by the expander as a positive contribution and the circulating pump duty $\dot{W}_p$ and the deep seawater pump duty $\dot{W}_d$ as negative contributions. A significative deep seawater pump consumption usually characterises OTEC plants because the cold water is drawn out at depths of 800–1000 m, so pumping loss is significantly high. According to the OTEC modelling proposed in [30], the deep seawater pump power can be expressed as the power necessary

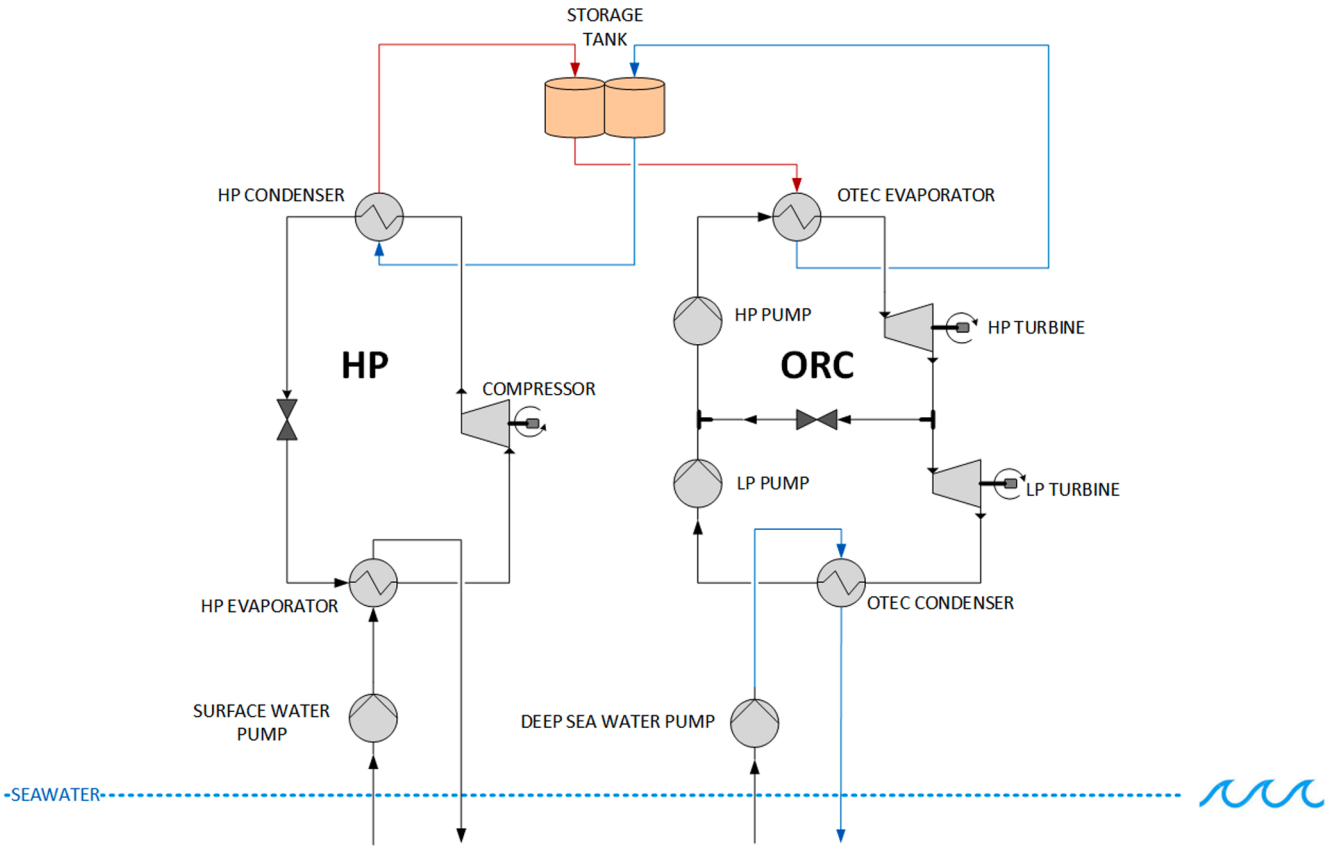

Fig. 5. Recuperated ORC without ocean re-injection.

to provide the head caused by the pressure drop Δp, calculated as shown in Equation (4):

$$\Delta p = f_D \rho L \frac{v^2}{2D} (Pa);\ \dot{W}_d = \frac{\dot{V}_d}{\eta_P} \Delta p\ (W) \tag{4}$$

where L is the extraction duct length, ρ is the seawater density, v the velocity inside the duct, D is hydraulic diameter, f_D is the Darcy's friction factor evaluated with the Colebrook equation solved by the Moody approximation considering a fully developed and turbulent flow regime (assumption valid also for off-design conditions), $\dot{V}_d$ the pumped volumetric mass flow rate and η_P the pump efficiency. The calculation of the pumping losses do not consider bending losses. As for the discharging phase, the charging electric power $\dot{W}_{ch}$ is given by the sum of the negative contributions of the compressor power and the surface water re-injection pump power.

It should be noted that for standard PTES configurations in which the charging cycle, the TS and the discharging cycle are arranged in series, the round trip efficiency is given by the product between the single cycles performance indicators, i.e. the first law efficiency η_{OTEC} for discharging phase, and the performance coefficient COP for the charging phase realised by the HP (Equation (5). This equation is effective if we consider the sources *iso*-thermal during the charging and discharging processes [13], so it will not be effective for the ORC with ocean re-injection configuration, as discussed in the results section.

$$\eta_{rt} = \eta_{OTEC} \mathrm{COP} \tag{5}$$

The storage volume V_s is evaluated by applying the mass conservation law to the tank. Starting from the ORC nominal evaporation duty, $\overline{\dot{Q}}_{evap}$ and its ΔT_{evap}, the nominal mass flow rate in the storage system $\overline{\dot{m}}_{st}$ is defined (Equation (6). V_s is then calculated (Equation (7) by including the charging time τ_{ch} and the water density ρ_w and the mass flow rate $\overline{\dot{m}}_s$. Finally, the storage model does not consider thermal losses because they are negligible due to the high volume-over-area ratio of the tank.

$$\dot{m}_{st} = \frac{\overline{\dot{Q}}_{evap}}{c_P \Delta T_{evap}} (kg/s) \tag{6}$$

$$V_s = \frac{\overline{\dot{m}}_s \tau_{ch}}{\rho_w} (m^3) \tag{7}$$

3.2. Numerical optimisation

3.2.1. Fluid packages

Numerical simulations are realised through the software Aspen Hysys V10. The system is modelled using the equation of states implemented in the software fluid packages. Seawater is considered as a mixture with H_2O and NaCl with a molar fraction of 0.004, and the fluid package used is Electrolyte NRTL [33]. RefProp was instead used for ammonia [34]. An overall optimisation is realised with the BOX algorithm, already implemented in Aspen. This is a sequential search algorithm suitable for highly non-linear problems [35].

3.2.2. Objective function

The objective function f_{obj} is the round trip efficiency η_{rt} maximisation (Equation (8):

$$f_{obj} = \max(\eta_{rt}) \tag{8}$$

The optimisation variables are OTEC evaporation pressure, OTEC condensation outlet temperature, OTEC condensation pressure, OTEC turbine inlet temperature, OTEC turbine output power, HP evaporation temperature, HP ΔT lift, and HP condensation outlet temperature. The main constraints are summarised in the following list:

- OTEC heat exchangers $\Delta T \geq 2$ K

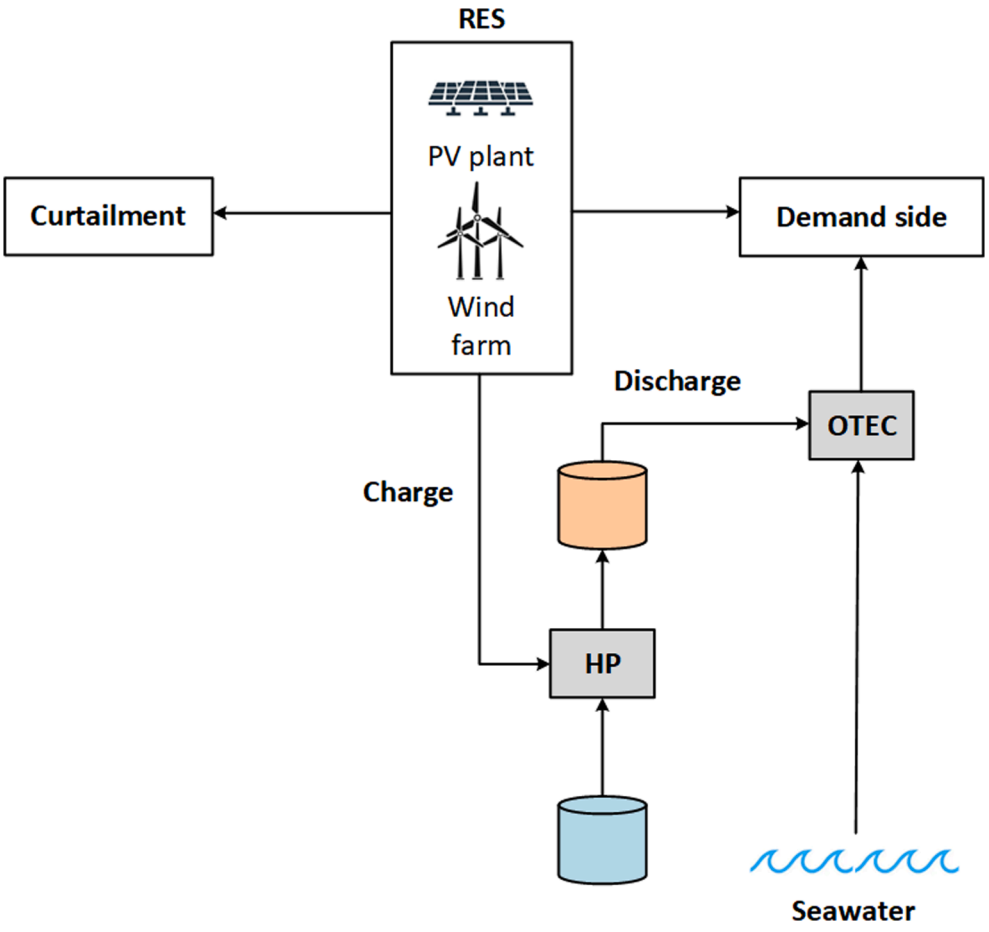

Fig. 6. Application to a realistic scenario.

- HP heat exchangers $\Delta T \geq 3$ K
- OTEC super-heating ≥ 2 K
- OTEC net output power = 10 MW ± 50 kW

3.2.3. Simulated cases

Numerical simulations allow the mapping of the η_{rt} in a defined storage temperature T_s range. Twelve simulations are realised for each plant configuration. In the first configuration (simple ORC with ocean re-injection) T_s varies from 40 °C to 60 °C. For every T_s different discharging ΔT on the OTEC evaporator, ΔT_{evap}, are considered. Regarding the other configurations (ORC and recuperated ORC without ocean re-injection), different HP temperatures at the condenser inlet, $T_{in,cond}$, are considered, ranging from 40 to 60 °C. For each of these, four different charging ΔT on the HP condenser ΔT_{cond} (equal to the OTEC discharging ΔT_{evap}) are investigated so that the considered T_s range varies from 45 °C to 80 °C. Table 2 summarises the simulated cases. By considering these temperature combinations, it is essential to keep in mind that for the ORC with ocean re-injection configuration, the charging and discharging ΔT realised across the HP condenser and the OTEC evaporator, respectively, are not equal, so Equation (5) cannot be considered for η_{rt} evaluation.

The results of this preliminary analysis aimed to define the optimal design (details in Section 4.1) highlight that the system layout with the simple ORC (without regeneration) and without ocean re-injection is the most performing in terms of η_{rt} and TS volume. The following part-load analysis and economic analysis (Section 4.1.4 and Section 4.1.5) are then performed only for the cited layout, considering the TS outlet temperature T_s equal to 50 °C with a corresponding TES volume of 100000 m^3 (values corresponding to the maximum achieved η_{rt}).

3.3. Part-load modelling

The thermodynamic analysis helps define the optimal design of the charging and discharging cycles. Nevertheless, the system will hardly work at design conditions during its operational life. When the system is integrated into a possible context that includes energy production from renewables and variable demand, the components will often face off-design conditions. A part-load analysis is then performed to evaluate these effects, mapping the performances of the components when the mass flow rate coming from the TES is reduced up to 20 % of its nominal value. The following sections provide the modelling equations of the part-load of components involved in the charging and discharging cycles.

3.3.1. Heat exchangers

The part-load modelling of the heat exchangers (i.e. condenser and evaporator) implies the evaluation of the exchanged heat flow rate $\dot{Q}$ in off-design conditions, as shown in Equation (9), where the overall heat transfer coefficient is given as in Equation (10), considering a flat surface for the heat exchange with negligible conductivity.

$$\dot{Q} = U_{off} A \Delta T_{ML} (W) \tag{9}$$

$$U_{off} = \frac{1}{\frac{1}{h_{i,off}} + \frac{1}{h_{e,off}}} \left(\frac{W}{m^2 K}\right) \tag{10}$$

where $h_{i,off}$ and $h_{e,off}$ indicate the heat exchanger coefficient for seawater flowing into the shell and ammonia flowing into tubes, respectively. A set of empirical correlations is used to estimate the heat transfer coefficients. The off-design coefficients, h_{off}, is evaluated basing on [36]

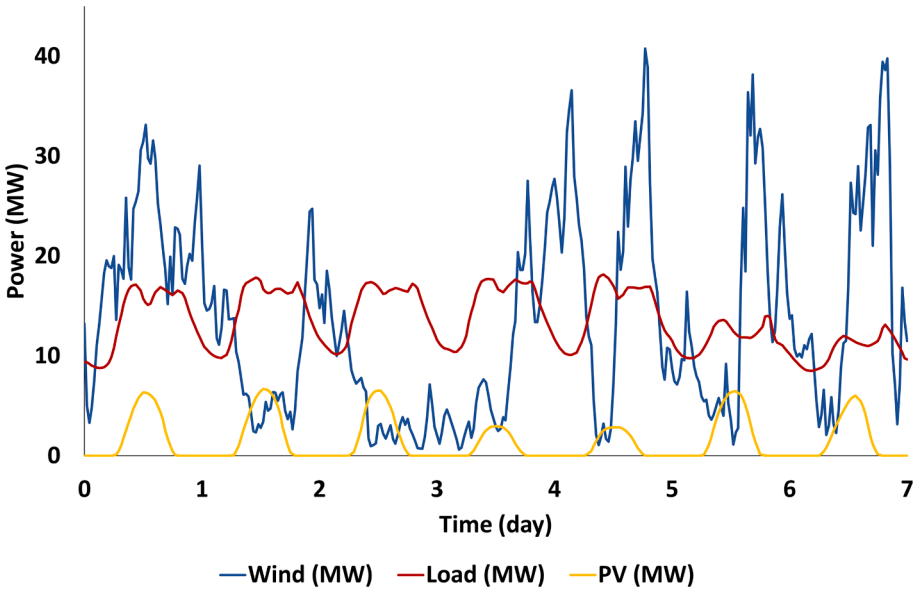

Fig. 7. RES production and load profile for the reference case study.

(Equation (11), where the design coefficient for H_2O, $h_{d,H2O}$, is given by the Dittus-Boelter correlation in Equation (12), considering *Re* as the Reynolds number and *Pr* as the Prandtl number. Since ammonia is involved in two-phase phenomena due to condensation and evaporation phases, h_{d,NH_3} cannot be evaluated with Dittus-Boelter. Instead of it, the experimental curve shown in [37] is used to calculate the value. Once the convective coefficients are calculated with the described methodology, the global heat exchanger coefficient $(UA)_{off}$ is known calculated from, considering the area A obtained by the preliminary thermodynamic analysis.

$$h_{off,H_2O} = h_{d,H_2O}\left(\frac{\dot{m}_{off}}{\dot{m}_d}\right)^{0.8}\left(\frac{W}{m^2K}\right) \tag{11}$$

$$Nu = \frac{hD}{k} = 0,0023Re^{0.8}Pr^{0.4} \tag{12}$$

Besides the heat transfer coefficients, pressure drops are an impacting parameter on the part-load performances of the heat exchangers. The off-design pressure drop Δp_{off} is calculated through the Darcy–Weisbach equation under the assumption of fully developed turbulent transient regime as in Equation (13), where ρ_{off} and ρ_d represents the density in off-design and design conditions, respectively.

$$\Delta p_{off} = \Delta p_d\left(\frac{\dot{m}_{off}}{\dot{m}_d}\right)^2\frac{\rho_d}{\rho_{off}}(Pa) \tag{13}$$

3.3.2. Turbine

The turbine off-design analysis aims to determine the influence of the part load on the *iso*-entropic efficiency. The experimental correlation given in [38] is suitable for ORC axial turbines working in part-load, so it is used in this case study as follows:

$$\frac{\eta}{\eta_D} = a + b\left(\frac{\Delta h}{\Delta h_D}\right) + c\left(\frac{\Delta h}{\Delta h_D}\right)^2 + d\left(\frac{\dot{V}_{out}}{\dot{V}_{out,D}}\right) + e\left(\frac{\dot{V}_{out}}{\dot{V}_{out,D}}\right)^2 + f\left(\frac{\Delta h}{\Delta h_D}\right)\left(\frac{\dot{V}_{out}}{\dot{V}_{out,D}}\right) \tag{14}$$

where *a, b, c, d, e* and *f* are coefficients depending on the number of stages, Δh is the enthalpy difference between inlet and outlet, $\dot{V}_{out}$ is the volume flow rate, which is known from the part-load condition, and the subscript *D* refers to the design conditions. The determination of the Δh in off-design conditions implies assessing the expansion ratio β. β is calculated through Equation (15) based on [39], which reports the relationship β-$\dot{m}_c$ of a real-world turbine working with similar conditions. The correct mass flow rate $\dot{m}_c$, which is known starting from the actual mass flow rate $\dot{m}$ and to the inlet conditions pressure and temperature, p_{in} and T_{in}, respectively, as expressed in Equation (16).

$$\dot{m}_c = \frac{\dot{m}\sqrt{T_{in}}}{p_{in}}(m \bullet s\sqrt{K}) \tag{15}$$

$$\dot{m}_c = a_0 + a_1 e^{[a_2 n_t^{a_3}(\beta-1)]} \tag{16}$$

where a_0, a_1, a_2, a_3 are experimental coefficients and n_t is the rotational speed, equal to 3000 rpm for this calculation. Given then the calculated β and the inlet conditions (p_{in} and T_{in}) is possible to calculate the Δh in off-design conditions.

Table 2
Simulated cases for a) Simple ORC with ocean re-injection. Non-bold values represent the re-injection temperature of the seawater; b) Simple or recuperated ORC without ocean re-injection. Non-bold values represent the storage temperature T_s.

Simple ORC with ocean re-injection (a)						Simple or recuperated ORC without ocean re-injection (b)					
	ΔT_{evap}						ΔT_{cond}				
T_s		5	10	15	20	$T_{in,cond}$		5	10	15	20
	40	35	30	25	20		**40**	45	50	55	60
	50	45	40	35	30		**50**	55	60	65	70
	60	55	50	45	40		**60**	65	70	75	80

3.3.3. Pumps

The pumps involved in the process are the OTEC circulation pump and the cold seawater pump. The off-design conditions are modelled using the mass flow rate-hydraulic head correlation curve and the mass flow rate-efficiency curve provided by Aspen Hysys (see [40] for further details). Both pumps are over-sized (15 % and 20 % respectively) as a precautionary approach. Pressure drops are not included in the model of the circulating pump since they are not impacting. Huge pressure drops characterise the deep seawater pump due to the extraction depth, which is not negligible, while localised pressure drops are neglected. The Darcy–Weisbach equation (Equation (13) provides the additional pump duty in off-design conditions.

3.3.4. Heat pump

Since the HP size required by design is not commercially available, the HP is modelled considering smaller modules working in parallel and turning on gradually as the load increases so that the TS outlet temperature is always 50 °C. The part load is then not meaningful in this case. Nevertheless, varying the load implies a changing water inlet temperature at the HP condenser with ΔT up to 15 °C so that the COP is influenced. To consider the effects of the changing temperatures of the sources on the COP, the Lorentz Coefficient Of Performance, $COP_{Lorentz}$ is introduced as suggested in [41].

$$COP_{Lorenz} = \frac{\frac{t_{sink,\,out} - t_{sink,\,in}}{\ln\left(\frac{t_{sink,\,out}+273{,}15\,^{\circ}C}{t_{sink,\,in}+273{,}15\,^{\circ}C}\right)}}{\frac{t_{sink,\,out} - t_{sink,\,in}}{\ln\left(\frac{t_{sink,\,out}+273{,}15\,^{\circ}C}{t_{sink,\,in}+273{,}15\,^{\circ}C}\right)} - \frac{t_{source,\,in} - t_{source,\,out}}{\ln\left(\frac{t_{source,\,in}+273{,}15\,^{\circ}C}{t_{source,\,out}+273{,}15\,^{\circ}C}\right)}} \tag{17}$$

where $t_{sink,in}$ and $t_{sink,out}$ are the hot source (the TS water) inlet and outlet temperatures, respectively, while $t_{source,in}$ and $t_{source,out}$ the cold source (the surface seawater at the HP evaporator) inlet and outlet temperatures. Considering the variations in the temperatures of the cold source and that $t_{sink,out}$ the TS temperature fixed to 50 °C, the only varying quantity is $t_{sink,in}$. Starting from the hot and cold source temperatures, the real COP, COP_r, is given by the Equation (18), where η^{II} is the HP second law efficiency calculated at the design conditions and equal to 0.46.

$$COP_r = \eta^{II} COP_{Lorentz} \tag{18}$$

3.4. Application in a realistic scenario

Once the system performances are assessed for every working condition, the plant potentialities are evaluated by simulating a weekly scenario, including the electric grid and generation from renewables (photovoltaic modules and wind turbines as described in Section 2.6).

The simulation has been realised considering a timestep t of 30 min, in which the interactions between the plant and grid, generation and users are constant over that period. The TS behaviour is then modelled analytically, solving its dynamic equations, as described in the following section.

3.4.1. TES energy and mass balances

Including energy and mass balances on the TES is helpful to evaluate the water volume charged or discharged in the two tanks (hot and cold) at every timestep. It is assumed that charging and discharging phases never co-occur, so the mass balance is defined in Equation (19), where V and ρ are the volume and mass density (assumed constant), respectively and $\dot{m}_{in}$ the mass flow rate entering the TS.

$$\frac{d(V\rho)}{dt} = \dot{m}_{in}(kg/s) \tag{19}$$

Integrating Equation (19) with the finite differences method between the timestep n and $n + 1$ the water volume stored is given by the Equation (20), where Δt is the timestep of 30 min and $V(t_{n+1})$ and $V(t_n)$ the volume computed at timestep $n + 1$ and n, respectively.

$$V(t_{n+1}) = V(t_n) + \frac{\dot{m}_{in}}{\rho}\Delta t\left(m^3\right) \tag{20}$$

Combining the energy balance shown in Equation (21) and the mass balance of Equation (20) is then possible to calculate the TS temperature at every timestep, as shown in Equation (22).

$$\rho c V(t)\frac{dT}{dt} + \rho c T(t)\frac{dV}{dt} = \dot{m}_{in}h_{in}(W/K) \tag{21}$$

$$\rho c V_n \frac{T_n - T_{n-1}}{\Delta t} + cT_n\dot{m}_{in} = \dot{m}_{in}h_{in}(W/K) \tag{22}$$

where c is the specific heat, T is the temperature and h_{in} the inlet enthalpy.

3.4.2. Decision paradigm

Charging and discharging phases are regulated by specifically imposed decision paradigms summarised as follows:

- The charging phase occurs if Renewable Energy Sources (RES) production is higher than the demand and:
  - o The hot TS tank is not completely charged;
  - o The charging power rate is higher than 500 kW, equal to the size of a single module of the HP. This assumption is reasonable, assuming the HP is working only if at least one module is working at the design power rate; if the charging rate is higher than the HP maximum nominal power (4,7 MW), the TS is charged at the nominal power.
- The discharging phase occurs when RES production is lower than the electric demand and:
  - o The hot TS is not out of charge;
  - o The required heat flow rate can let the OTEC work with a part load in the 20% − 100% of the nominal mass flow rate flowing into the OTEC evaporator. If the required discharging power rate is higher than the OTEC nominal size (10 MW), the discharge occurs at 10 MW; on the contrary, if it is lower than the 20 % part load, the discharge occurs at that value.

In addition, when the demand is higher than the RES production, but the TS is not able to discharge because of one of the situations described above, it is possible to let the OTEC work in its traditional configuration, bypassing the HP and TS. In this case, the electric production is obtained from the natural ΔT between the surface and deep water. This particular discharge configuration, then, occurs if these conditions occur simultaneously:

- The electric demand is higher than 0;
- The TES discharging is not available;
- The required discharging rate is in the range of 50–100 % of the OTEC nominal power (2,67 MW).

3.5. Economic analysis

3.5.1. Levelised cost of storage

The economic performance indicators are assessed by calculating the LCOS, the typical parameter used to compare the competitiveness of different storage technologies. Its definition, shown in Equation (23), takes into account the investment costs (CAPEX), the operational costs (OPEX), and the charging cost, including a discount rate r and considering an operating life of N years.

$$LCOS = \frac{Investement\ cost + \sum_n^N \frac{O\&M}{(1+r)^n} + \sum_n^N \frac{Charging\ cost}{(1+r)^n} + \frac{End\ of\ life\ cost}{(1+r)^{N+1}}}{\sum_n^N \frac{E_{dis}}{(1+r)^n}}(€/Wh) \tag{23}$$

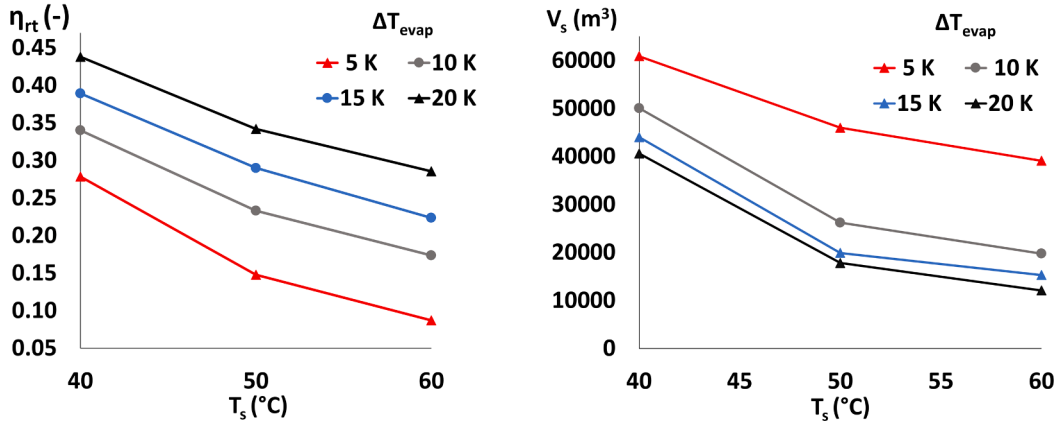

Fig. 8. ORC with ocean re-injection configuration. Round-trip efficiency varying the storage temperature T_s and the discharging temperature difference ΔT_{evap} (left). Storage volume varying T_s and ΔT_{evap} (right).

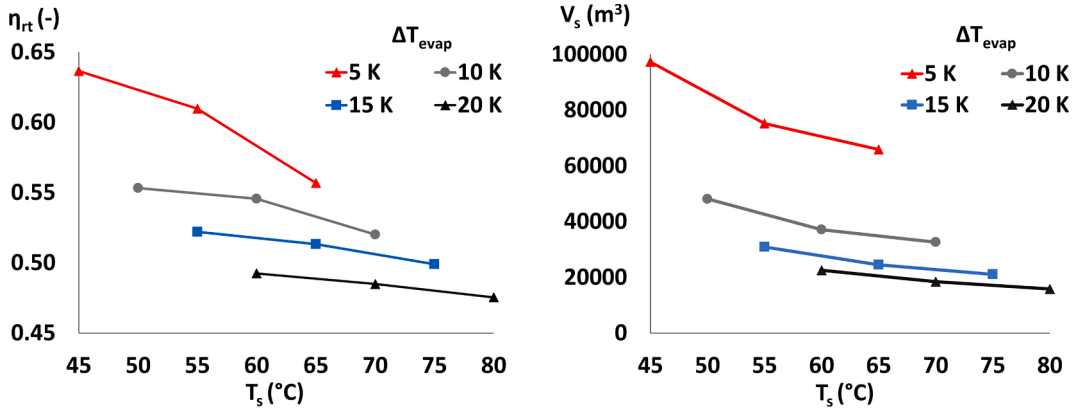

Fig. 9. ORC without ocean re-injection. Round-trip efficiency varying the storage temperature T_s and the OTEC discharging ΔT_{evap} (left). Storage volume varying $T_{in,cond}$ and the OTEC discharging temperature difference ΔT_{evap} (right).

where:

- The investment cost is calculated as the ratio between the CAPEX (the sum of the investment cost of the components) and the Capital Recovery Factor (CRF), defined in Equation (24) as a function of n and interest rate i (7 %)

$$CRF = \frac{i(1+i)^n}{(1+i)^n - 1} \tag{24}$$

- O&M includes operational costs and maintenance, calculated as 2,5 % of the CAPEX and the annual cost for the chlorine injection to prevent bio-fouling in the heat exchangers. The latter is evaluated based on typical yearly maintenance values for boi-fouling prevention for heat exchangers (2€/(m^3/h)) provided by [42];
- *End of life costs* is not considered since this study evaluate a preliminary economic analysis and not a life cycle assessment;
- E_{dis} is the discharged energy. This term includes the TS discharging phases and the OTEC discharging phases working bypassing the HP and the TS;
- The discount rate *r,* equal to 7%*;*
- The plant operational life N is assumed to be equal to 20 years, based on typical values for ORC plants;
- Charging costs are equal to 0 because the charging phases are realised only with the RES surplus.

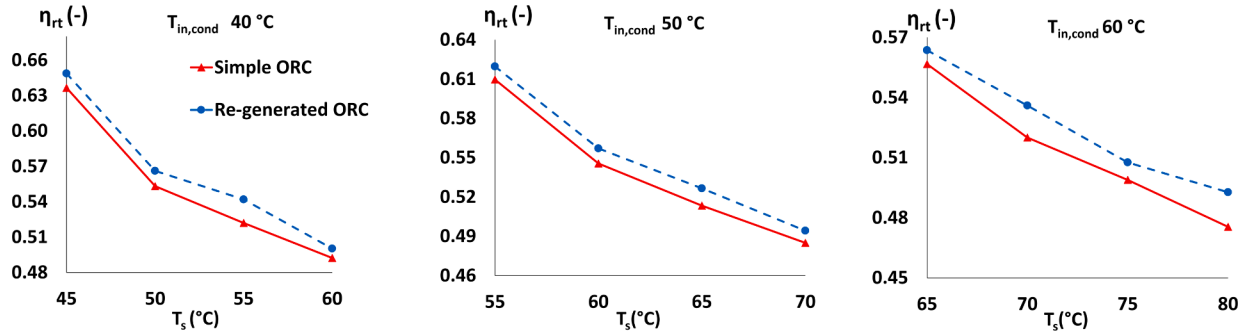

Fig. 10. Round-trip efficiency for the recuperated ORC without ocean re-injection.

3.5.2. CAPEX

The Capital Expenditures (CAPEX) calculation for the HP evaporator, pumps (OTEC pump and cold seawater pump), compressor and turbine is based on the methodology described in [43]. The referring costs are updated to 2018 through the Chemical Plant Index $CEPCI_{2018}$ and the medium €/$ change factor f_{2018}. The total CAPEX is given by the sum of the investment cost of the single components $CAPEX_i$, as expressed in Equation (25).

$$CAPEX_i = \frac{1.18}{f_{2018}} \frac{CEPCI_{2018}}{CEPCI_{1995}} C^0_{p,i} F_{BM,i} (€) \quad (25)$$

where $C^0_{p,i}$ is the *i-th* component cost and F_{BM} is the bare module factor, which considers the component material an operation pressure, $F_{p,i}$ and $F_{M,i}$ respectively. $C^0_{p,i}$ is calculated using the component size parameter A_i (i.e. the area for heat exchangers and the nominal power for turbines and compressors), and the factors $K_{1,i}$, $K_{2,i}$ and $K_{3,i}$ depending on the component.

$$log_{10} C^0_{p,i} = K_{1,i} + K_{2,i} log_{10} A_i + K_{3,i} (log_{10} A_i)^2 \quad (26)$$

$C^0_{p,i}$ is then corrected with two correction parameters that contribute to the final cost: $F_{p,i}$ to consider the operating pressure, and $F_{M,i}$ to consider the material. The overall factor F_{BM} takes into account both $F_{p,i}$ and $F_{M,I}$ and is given in Equation (27), using B_1 and B_2 as specific coefficients depending on the component. While $F_{M,i}$ only depends on the material, $F_{p,i}$ also depends on the operational pressure $p_{g,i}$ and some specific coefficients C_1, C_2 and C_3, as shown in Equation (28).

$$F_{BM,i} = B_1 + B_2 F_{p,i} F_{M,i} \quad (27)$$

$$log_{10} F_{p,i} = C_{1,i} + C_{2,i} log_{10} p_{g,i} + C_{3,i} (log_{10} p_{g,i})^2 \quad (28)$$

Equations (26), (27) and (28) are also used for the cost estimation of shell and tube heat exchangers, which are among the most used heat exchangers for OTEC applications [30]. Even if the size exceeds the recommended operational range, the cost has been linearly extrapolated. An increase of 50 % has been applied to consider extra costs like transportation and placement.

Since a dismissed oil tanker is used as the TS, the CAPEX is estimated using reference costs reported on [44]. The price of the reference has been increased by 50 % to consider the refitting of the oil tanker and the installation of the off-shore platform and the pipes.

4. Results and discussion

4.1. Preliminary thermodynamic analysis

4.1.1. ORC with ocean re-injection

Fig. 8 shows the round-trip efficiency varying with the storage temperature T_s. The effects of the thermal integration given by the ocean gradient are visible, since the round-trip efficiency η_{rt} increases with ΔT_{evap}, i.e., as the temperature of the re-injected water decreases. As previously discussed, the cold source (cold seawater) is at a temperature $T_c < T_{surf}$, so that it can be considered a thermal integration. During the discharging phase, the system takes advantage of both the ΔT realised by the HP from T_{surf} to T_s, and the ΔT between the ocean re-injection temperature, T_s-ΔT_{evap}. When ΔT_{evap} is high, then, the water is re-injected at a lower temperature, and the thermal losses are reduced, increasing the overall efficiency. Basing on this result discussion, the highest η_{rt} is then reached with the maximum ΔT_{evap} (20 °C). Despite the benefits of the thermal integration, the efficiency achieved with this layout (45%) is in the lower bound of the typical η_{rt} efficiencies of TI-PTES [45]. The low performance is due to the high ΔT covered (thus the high compressor duty) by the HP the move the heat from T_{surf} to T_s. For each considered ΔT_{evap}, then, the higher is the T_s, the lower is the efficiency. On the other hand, higher storage temperatures significantly reduce tank volume since the storage energy density is enhanced. In addition, T_s, V_s decreases as ΔT_{evap} increases, due to the pinch point constraint and the consequent increase in the temperature at which water is discharged after the evaporator.

At the end of this analysis, it is clear that the two considered KPIs have an opposite behaviour, so the choice of the storage temperature level is a trade-off between the efficiency and the storge bulk. Given the peculiarities of the analysed case study, storage capacities up to 150000 m3 can be hosted in the cargo ship capacity, so efficiency can be prioritised.

4.1.2. ORC without ocean re-injection

The limitations of the previous architecture can be overcome by non re-injecting the water into the ocean. The configuration without ocean re-injection can exploit the thermal integration better, since the tem-

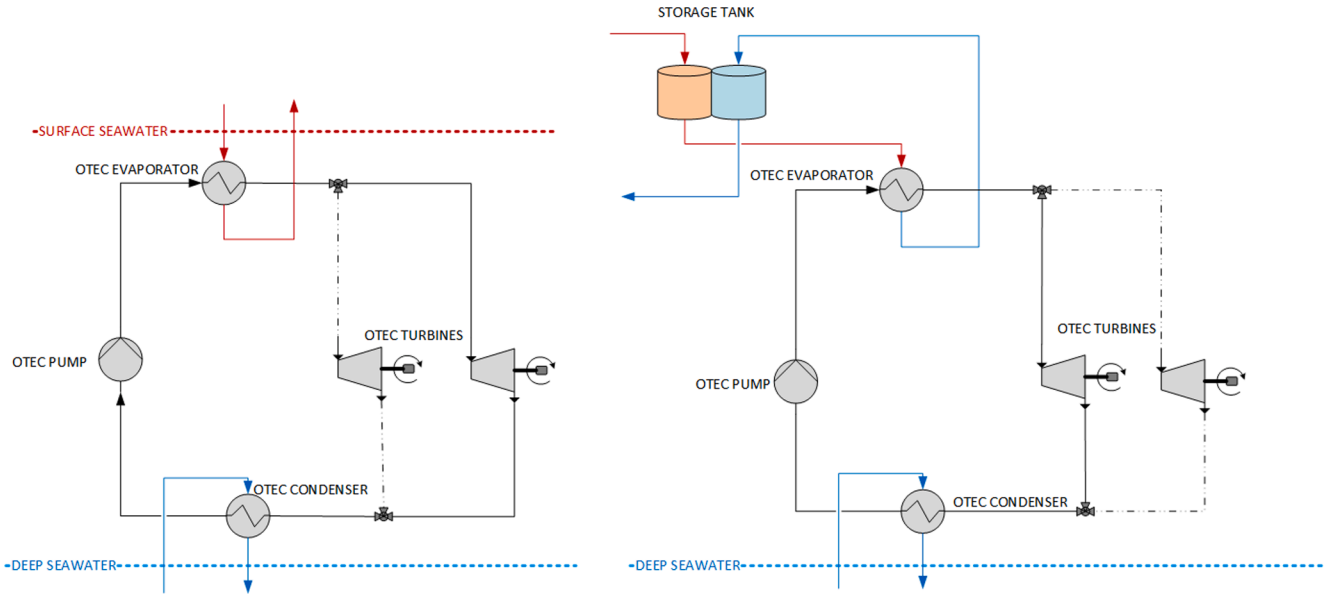

Fig. 11. System layout with two turbines. On the right side the configuration as simple OTEC, while on the left side the discharging cycle of the integrated PTES-OTEC.

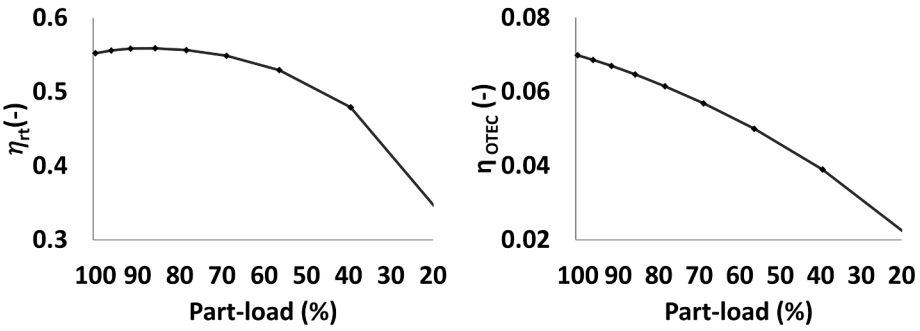

Fig. 12. Round trip efficiency (left) and OTEC first law efficiency (right) varying the part-load conditions. Part load conditions on the x-axis refer to the mass flow rate flowing through the OTEC evaporator.

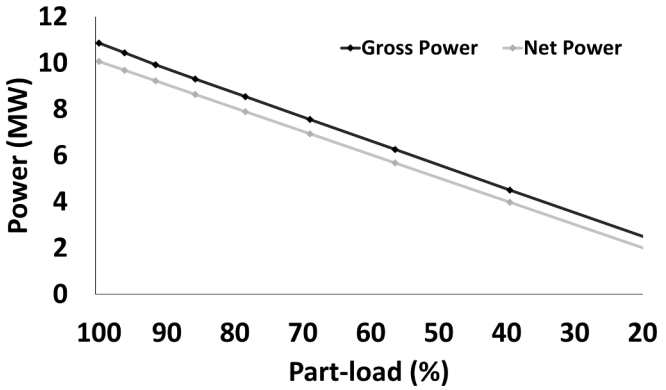

Fig. 13. Turbine *iso*-entropic efficiency (left side) and OTEC output power with part-load conditions. Part load conditions on the x-axis refer to the mass flow rate flowing through the OTEC evaporator.

perature difference from T_{surf} to T_s is partially used for the evaporation phase of the ORC, and the remaining part is not wasted but stored in the additional tank. The contribution of the ocean gradient from T_{surf} to T_c is also still used for the condensation phase of the ORC. By doing so, the HP works with smaller ΔT (compared to the previous case) to move heat from one tank to another, so the COP increases. Since this layout is arranged in series as proposed in [13], the η_{rt} increases as well (Equation (5). As results show in Fig. 9, the round-trip efficiency decreases then when T_s increases for a given $T_{in,cond}$ since the HP performance worsens because of the higher compression duty. It should be noted that by comparing this configuration to the previous one, η_{rt} decreases as ΔT_{evap} enlarges. In conclusion, the lower ΔT_{evap} is, the higher is the initial storage tank temperature, and the higher is η_{rt} because of the COP reduction [16,18]. The benefits of the better exploitation of thermal integration finally reflect in the η_{rt}, which goes up to 64%, which is in agreement with the cited literature results.

Despite the benefits of round-trip efficiency, water reintegration in the TS from the OTEC evaporator implies the necessity to oversize the storage tank. In this configuration, the volume size is doubled compared to the previous case, so the two sections (hot and cold) are used alternatively for the charging and discharging phases. As shown in Fig. 9 (right), the storage volume decreases as T_s gets higher because the HP lift is enhanced; for equal T_s values, the volume is also reduced when ΔT_{evap} increases because of the inverse proportionality between the OTEC evaporator duty and ΔT.

As in the previous configuration, the storage volume is highly influenced by the selected storage temperature T_s, and the smallest value is achieved nearby the lowest efficiency. Still, the highest required tank volume can be hosted in a cargo ship. According to that, different bulk carrier sizes can be used as storage, from handymax up to Aframax, characterised by a capacity (deadweight) up to 120000 t. Eventually, the selection of the final storage size must take into account also some economic evaluations.

4.1.3. *Recuperated ORC without ocean re-injection*

Since the previous plant layout showed promising performances, it was worth investigation of some potential improvements of the efficiency of introducing regeneration in the ORC cycle. The vapour spill and recovery improves the OTEC cycle first law efficiency because the evaporation duty is reduced. This improvement determines the whole round-trip efficiency of the system increase, as described in Section 2.5.3. Nevertheless, η_{OTEC} growth is limited to 0.5 % in most cases due to the small available temperature difference between the evaporator and condenser. η_{rt} increase is limited to 1–2 % also because the HP performance is unchanged (Fig. 10). The round-trip efficiency varies with T_s and ΔT_{evap} as in the previous configurations. By increasing the storage temperature T_s the recuperated cycle benefit is more evident. The consequent higher efficiency of this solution reduces the condenser duty, thus allowing the condensation at a lower temperature with a reduced

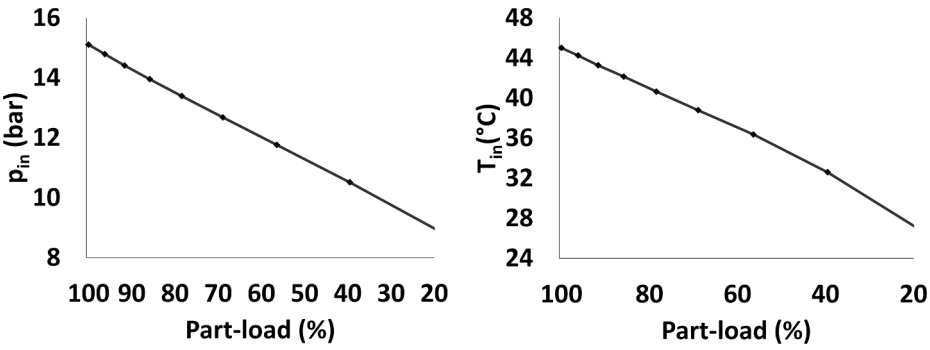

Fig. 14. Turbine inlet conditions varying the part-load. Turbine inlet pressure (left) and turbine inlet temperature (right). Part load conditions on the x-axis refer to the mass flow rate flowing through the OTEC evaporator.

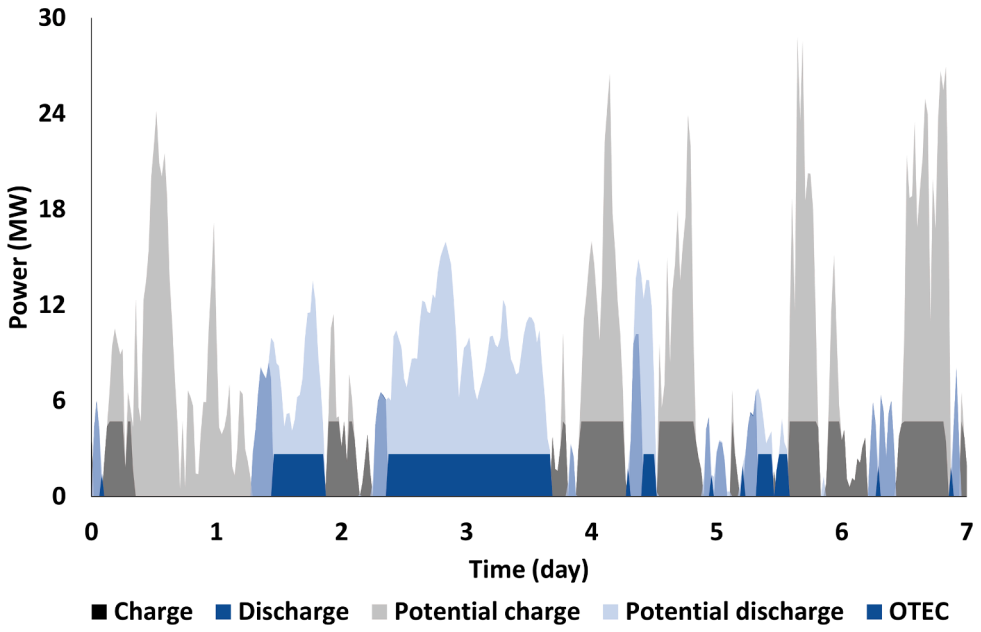

Fig. 15. Weekly simulation.

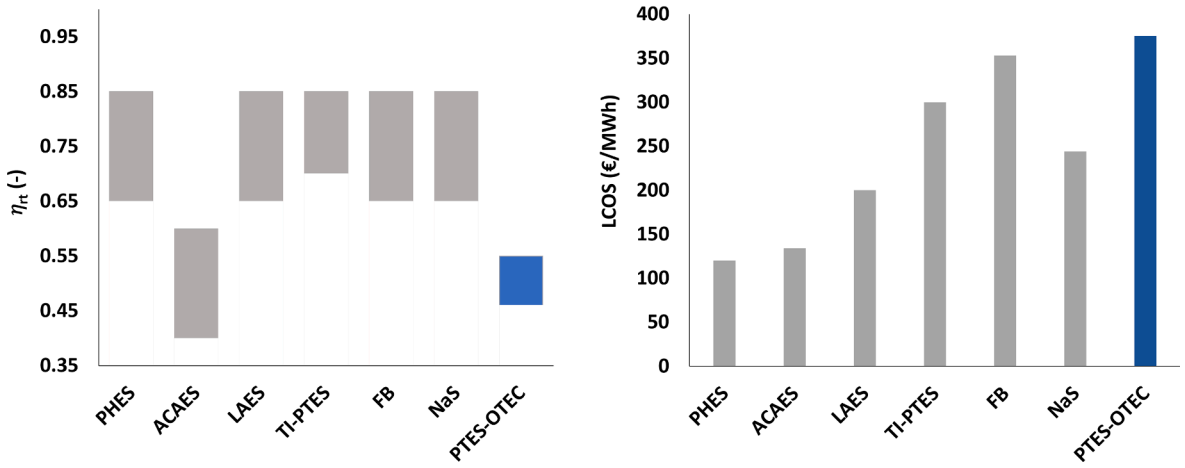

Fig. 16. Round-trip efficiency (left) and LCOS (right) for PTES-OTEC compared to other grid-scale storage technologies.

mass flow rate. The reduced mass flow rate limits the pressure drop and the pump loss of deep seawater. Ammonia spill and recovery cycle can also reduce the storage volume due to the higher efficiency and minor heat requested at the evaporator for the same discharged electric power. However, the recuperation contribution is insignificant, so volume reduction is limited to 500–1500 m^3 for each configuration. Because of the η_{rt} limited improvements, this configuration does not represent an interesting alternative, considering the additional cycle complication.

4.1.4. Part-load characterisation

Starting from the analysis discussed in the previous sections, only one configuration has been selected for the further off-design and economic analysis. Since the layout without ocean re-injection showed to be the most performing in terms of η_{rt}, the system architecture with two tanks (Fig. 4) is the one selected, not considering the ammonia spill recuperation which bring to a limited η_{rt} increase. The simple ORC without ocean re-injection is then consider from now one. Particularly, the selected Ts is of 50 °C, which is a configuration with a quite performing η_{rt}, equal to 50%, and a storage volume of around 100000 m^3, which is feasible using a cargo ship. Since for this application the system can work as an integrated PTES-OTEC or as a simple OTEC according to the requirements (Section 3.4.2 for details), an additional ORC turbine is necessary. Working as a simple OTEC, indeed, would determine significantly different mass flow rate of the working fluid too different from the working conditions designed for the turbine of the PTES-OTEC configuration. A reference scheme is showed in Fig. 11.

The part-load conditions affect the performance of the system, deteriorating its efficiency. As shown in Fig. 12, the round-trip efficiency varies broadly from 0.55 in the design conditions to 0.35 in the minimum mass flow rate capacity. The performance deterioration follows a turbine's classical *iso*-entropic efficiency tendency, in which there is a limited efficiency increment until the part load is 80–90 % of the nominal capacity and then permanently decreases (Fig. 13). In PTES systems, the turbine isentropic efficiency impacts the storage round trip efficiency significantly, which consequently deteriorates with the turbine efficiency tendency. Other parameters that significantly impact the η_{rt} are the OTEC are first law efficiency (Fig. 12 right), which constantly decreases with the part-load increase since this configuration refers to Equation (4), in which the round trip efficiency decreases proportionally to the OTEC efficiency. On the other hand, increasing the part load also

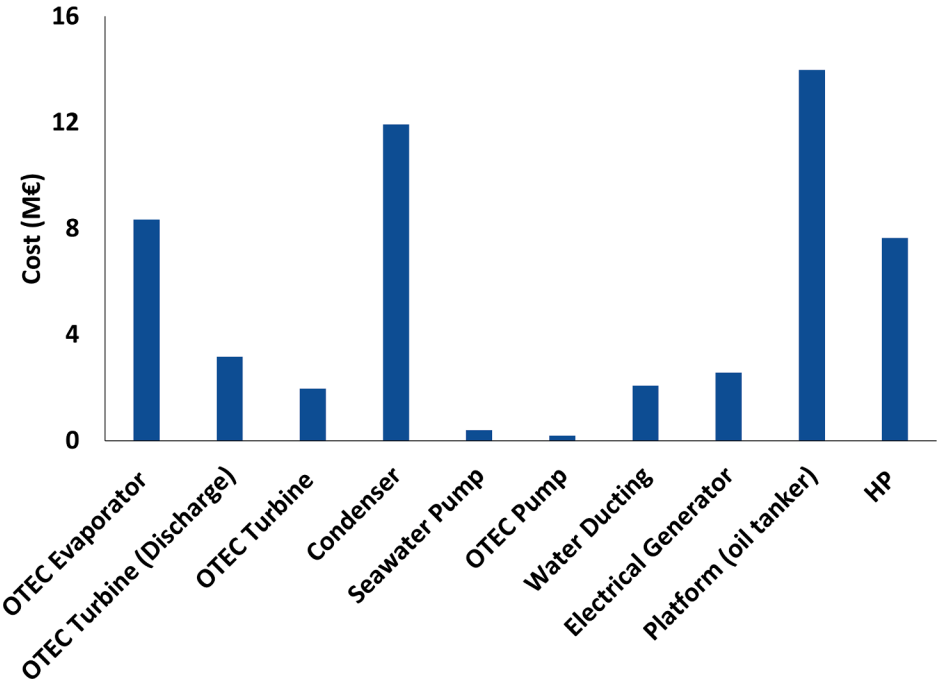

Fig. 17. CAPEX distributed over the components of the plant.

increases the HP COP because the compressor duty is reduced. Nevertheless, since the HP is modular, it hardly works in significative part-load conditions, so the COP changes do not significantly affect the round trip performance.

The part load behaviour considerably also affects the inlet conditions of the turbine and thus influences the overall operating conditions. Fig. 14 represents some representative turbine working parameters. When the mass flow rate drops until 20% of the nominal capacity, the turbine inlet pressure drops with it. Since the optimisation constraints impose a minimum superheating value, the turbine inlet temperature follows the pressure tendency in the same way. The turbine outlet pressure, instead, does not vary significantly during the off-design. All these contributions at the end decurtate the net power production, as shown on the right side of Fig. 13.

4.1.5. Operational behaviour

Because of the part-load characterisation, a simulation with a likely VRE production and user demand is possible. Results of the operative simulation are shown in Fig. 15, in which the interactions within the storage, production and load are visible during a week-time sample. The figures emphasise the light-coloured areas, representing the charging/discharging potentialities (i.e. the charging/discharging requests according to the control strategy). These areas are broad compared to the dark-coloured areas, representing the actual time intervals in which the plant is working, charging, or discharging or as a simple OTEC plant. This behaviour indicates that the plant operates with a limited number of equivalent hours, mainly due to the limitations imposed by the charging/discharging size and storage capacity. Nevertheless, the following consideration can be stated:

- When energy is required (discharging phases), the system intervenes to discharge the TS when possible. When it is impossible, the standard OTEC configuration turns on, almost always covering part of the required load, unloading the electric grid and assuring an amount of the provided energy is fossil-free.
- When energy needs to be stored (energy surplus phases, charging configuration), the TS limits the system's stocking capacity. In this scenario, some particular situations in which there is a potential charge but the storage capacity is full can occur, so the surplus is curtailed, as happens during day 1 in Fig. 15).

4.1.6. LCOS and comparison with other ESS

Finally, the economic analysis places the proposed TI-PTES in the grid-scale storages overview to state its competitiveness with more mature technologies. Fig. 16 shows the LCOS obtained for the proposed OTEC-PTES system compared to the LCOS of other known storage technologies. The LCOS obtained is 388 €/MWh, similar to one of other batteries, such as RFB. It should be noted that the calculated LCOS refers to the sample week chosen for the simulation. The reported LCOS for other technologies are mean values [8], which include the uncertainty related to time sample simulation and load and generation curves, as well as the control strategies so that results can be affected by significative variation. Despite that, the PTES-OTEC application is kindly new, so this is the first value to be compared to known LCOS quantities to collocate this novel technology better. Furthermore, this LCOS considers the off-design conditions, which are often not considered during the LCOS calculations.

The high obtained LCOS is due to the low operational time (limited by the storage size), but it could be improved by integrating an optimised control strategy. In addition, the high LCOS is due to the increased investment cost derived from the high price of the components. Fig. 17 shows how the CAPEX is distributed over all the components. The most expansive contribution is given by the oil tanker, which is over 13 M€. Also, the OTEC heat exchangers (evaporator and condenser) have a significantly high cost because of the large exchanging area necessary to ensure the desired heat flow rate with limited minimum temperature differences (2–3 K as $\Delta T_{approach}$). The cost of the other components is in agreement with [22,30,44].

To complete the overview of ESS comparison, Fig. 15 also shows how this technology is comparable to the others in terms of round-trip efficiency. The η_{rt} ranging values from 45% to 55% refer to a sensitivity analysis obtained varying the load of ± 20%. Despite these are values lower than the other reported technologies η_{rt}, it should be noted that the proposed storage system is not significantly sensitive to self-discharge phenomena, thank the high volume over area ratio. Degradation phenomena also do not affect this storage, except for reversible

fouling issues in the heat exchangers. Finally, it should be considered that the reported values are strongly dependent on the simulation scenario and the consideration or not of the off-design conditions.

5. Conclusions

This paper investigates a novel Thermal Integrated-Pumped Thermal Energy Storage (TI-PTES) configuration which includes an Ocean Thermal Energy Conversion (OTEC) plant as the discharging phase. The proposed systems provides operational flexibility to the plant, which is able to exploit the natural contribution of solar radiation on the ocean in tropical regions, using an end-life cargo ship as a plant platform and storage. The resulting 20 MWh storage systems, categorisable as TI-PTES thanks to the free solar integration, have been preliminary analysed through a round trip optimisation to define the best plant layout and working conditions, particularly the storage temperature. Results highlight that the highest round trip efficiency of 64% is achieved by re-injecting the seawater into the storage tank, using it as two-sector storage, one for charge and of for discharge. The resulting storage volume is around 100000 m^3, which is significant to manage but is suitable for cargo ship available capacities.

The analysis has been further deepened by characterising the part-load performances of the components and then providing a simulation in real working conditions. The weekly simulation highlights that the system always guarantees an amount of energy produced by the OTEC, which ensures a contribution by fossil-free production. The medium round trip efficiency of 49% calculated during a weekly operation and counting of the off-design condition is also comparable with the other cited Energy Storage Systems (ESS) when off-design performances are embedded. The obtained Levelised Cost of Energy (LCOS) is slightly higher than other grid-scale storage technologies (388 $/MWh), even though this comparison is qualitative because of a strong uncertainty depending on the selected load, generation profile, and control strategies. Nevertheless, the investment costs are high and significantly dependent on the cargo ship cost, which can vary broadly depending on the re-structuration work. This is the reason why further analysis should focus also on the detailed economic characterisation of the storage tank into the cargo ship to better estimate its cost-effectiveness. As a future step of the analysis, further investigations should address the specific design of the storage tank inside the cargo ship. The thermodynamic analysis, then, highlights that the system is feasible since the thermal integration helps the storage to work with round trip efficiencies similar to the other investigated PTES. However, the results are based on the assumption of constant surface temperature, which is reasonable for the selected location (Panama). Further analysis should also address the impact of different temperature profiles of the thermal source.

CRediT authorship contribution statement

A. Ghilardi: Conceptualization, Data curation, Formal analysis, Investigation, Methodology, Software, Visualization, Writing – original draft. **A. Baccioli:** Conceptualization, Methodology, Writing – review & editing. **G.F. Frate:** Conceptualization, Writing – review & editing. **M. Volpe:** Data curation, Formal analysis, Investigation, Software. **L. Ferrari:** Conceptualization, Funding acquisition, Project administration, Supervision, Writing – review & editing.

Declaration of Competing Interest

The authors declare that they have no known competing financial interests or personal relationships that could have appeared to influence the work reported in this paper.

Data availability

Data will be made available on request.

References

[1] G.F. Frate, L. Ferrari, U. Desideri, Energy storage for grid-scale applications: Technology review and economic feasibility analysis, Renew. Energy 163 (2021) 1754–1772, https://doi.org/10.1016/j.renene.2020.10.070.

[2] M.C. Argyrou, P. Christodoulides, S.A. Kalogirou, Energy storage for electricity generation and related processes: Technologies appraisal and grid scale applications, Renew. Sustain. Energy Rev. 94 (2018) 804–821, https://doi.org/10.1016/j.rser.2018.06.044.

[3] M.M. Rahman, A.O. Oni, E. Gemechu, A. Kumar, The development of techno-economic models for the assessment of utility-scale electro-chemical battery storage systems, Appl. Energy 283 (2021), 116343, https://doi.org/10.1016/j.apenergy.2020.116343.

[4] E. Sánchez-Díez, E. Ventosa, M. Guarnieri, A. Trovò, C. Flox, R. Marcilla, et al., Redox flow batteries: Status and perspective towards sustainable stationary energy storage, J. Power Sources (2021) 481, https://doi.org/10.1016/j.jpowsour.2020.228804.

[5] O. Dumont, G.F. Frate, A. Pillai, S. Lecompte, M. De paepe, V. Lemort. Carnot battery technology: A state-of-the-art review. J. Energy Storage 32 (2020). 10.1016/j.est.2020.101756.

[6] E. Borri, A. Tafone, A. Romagnoli, G. Comodi, A review on liquid air energy storage: History, state of the art and recent developments, Renew. Sustain. Energy Rev. 137 (2021), 110572, https://doi.org/10.1016/j.rser.2020.110572.

[7] A. Benato, A. Stoppato, Pumped Thermal Electricity Storage: A technology overview, Therm. Sci. Eng. Prog. 6 (2018) 301–315, https://doi.org/10.1016/j.tsep.2018.01.017.

[8] A. Olympios, J. Mctigue, N. Renewable, P. Sapin, C.N. Markides, Pumped-Thermal Electricity Storage Based on Brayton Cycles (2021), https://doi.org/10.1016/B978-0-12-819723-3.00086-X.

[9] T. Desrues, J. Ruer, P. Marty, J.F. Fourmigué, A thermal energy storage process for large scale electric applications, Appl. Therm. Eng. 30 (2010) 425–432, https://doi.org/10.1016/j.applthermaleng.2009.10.002.

[10] R.B. Laughlin, Pumped thermal grid storage with heat exchange, J Renew Sustain Energy (2017) 9, https://doi.org/10.1063/1.4994054.

[11] W. Tian, H. Xi, Comparative analysis and optimization of pumped thermal energy storage systems based on different power cycles, Energy Convers. Manag. 259 (2022), 115581, https://doi.org/10.1016/j.enconman.2022.115581.

[12] O. Dumont, V. Lemort, Mapping of performance of pumped thermal energy storage (Carnot battery) using waste heat recovery, Energy 211 (2020), 118963, https://doi.org/10.1016/j.energy.2020.118963.

[13] G.F. Frate, M. Antonelli, U. Desideri, A novel Pumped Thermal Electricity Storage (PTES) system with thermal integration, Appl. Therm. Eng. 121 (2017) 1051–1058, https://doi.org/10.1016/j.applthermaleng.2017.04.127.

[14] G.F. Frate, L. Ferrari, U. Desideri, Multi-criteria investigation of a pumped thermal electricity storage (PTES) system with thermal integration and sensible heat storage, Energy Convers. Manag. 208 (2020), 112530, https://doi.org/10.1016/j.enconman.2020.112530.

[15] S. Hu, Z. Yang, J. Li, Y. Duan, Thermo-economic analysis of the pumped thermal energy storage with thermal integration in different application scenarios, Energy Convers. Manag. (2021) 236, https://doi.org/10.1016/j.enconman.2021.114072.

[16] G.F. Frate, L. Ferrari, U. Desideri, Rankine carnot batteries with the integration of thermal energy sources: A review, Energies (2020) 13, https://doi.org/10.3390/en13184766.

[17] G.F. Frate, A. Baccioli, L. Bernardini, L. Ferrari, Assessment of the off-design performance of a solar thermally-integrated pumped-thermal energy storage, Renew. Energy 201 (2022) 636–650, https://doi.org/10.1016/j.renene.2022.10.097.

[18] A.V. Olympios, J.D. McTigue, P. Farres-Antunez, A. Tafone, A. Romagnoli, Y. Li, et al., Progress and prospects of thermo-mechanical energy storage—a critical review, Prog. Energy 3 (2021), 022001, https://doi.org/10.1088/2516-1083/abdbba.

[19] Renewable Energy Agency I. OCEAN THERMAL ENERGY CONVERSION ABOUT IRENA. 2014.

[20] J. Langer, A.A. Cahyaningwidi, C. Chalkiadakis, J. Quist, O. Hoes, K. Blok, Plant siting and economic potential of ocean thermal energy conversion in Indonesia a novel GIS-based methodology, Energy (2021) 224, https://doi.org/10.1016/j.energy.2021.120121.

[21] G. Lopez, M.D. Ortega Del Rosario, A. James, H. Alvarez. Site Selection for Ocean Thermal Energy Conversion Plants (OTEC): A Case Study in Panama. Energies 15 (2022), 3077. 10.3390/en15093077.

[22] S.M. Masutani, P.K. Takahashi, Ocean Thermal Energy Conversion (otec), Encycl. Ocean Sci., Elsevier (2001) 1993–1999, https://doi.org/10.1006/rwos.2001.0031.

[23] W. Liu, X. Xu, F. Chen, Y. Liu, S. Li, L. Liu, et al., A review of research on the closed thermodynamic cycles of ocean thermal energy conversion, Renew. Sustain. Energy Rev. 119 (2020), 109581, https://doi.org/10.1016/j.rser.2019.109581.

[24] P. Bombarda, C. Invernizzi, M. Gaia, Performance analysis of OTEC plants with multilevel organic rankine cycle and solar hybridization, J. Eng. Gas Turbines Power 135 (2013) 1–9, https://doi.org/10.1115/1.4007729.

[25] M.Z.Z. Abidin, M.N.M. Rodhi, F. Hamzah, N.A. Ghazali, Assessing biofouling in Ocean Thermal Energy Conversion (OTEC) power plant – A review, J. Phys. Conf. Ser. (2021) 2053, https://doi.org/10.1088/1742-6596/2053/1/012011.

[26] M. Wang, R. Jing, H. Zhang, C. Meng, N. Li, Y. Zhao, An innovative Organic Rankine Cycle (ORC) based Ocean Thermal Energy Conversion (OTEC) system with performance simulation and multi-objective optimization, Appl. Therm. Eng. 145 (2018) 743–754, https://doi.org/10.1016/j.applthermaleng.2018.09.075.

[27] F. Yilmaz, Energy, exergy and economic analyses of a novel hybrid ocean thermal energy conversion system for clean power production, Energy Convers Manag 196 (2019) 557–566, https://doi.org/10.1016/j.enconman.2019.06.028.
[28] A. Khosravi, S. Syri, M.E.H. Assad, M. Malekan, Thermodynamic and economic analysis of a hybrid ocean thermal energy conversion/photovoltaic system with hydrogen-based energy storage system, Energy 172 (2019) 304–319, https://doi.org/10.1016/j.energy.2019.01.100.
[29] J. Bao, L. Zhao, A review of working fluid and expander selections for organic Rankine cycle, Renew. Sustain. Energy Rev. 24 (2013) 325–342, https://doi.org/10.1016/j.rser.2013.03.040.
[30] D. Vera, A. Baccioli, F. Jurado, U. Desideri, Modeling and optimization of an ocean thermal energy conversion system for remote islands electrification, Renew. Energy 162 (2020) 1399–1414, https://doi.org/10.1016/j.renene.2020.07.074.
[31] E. Macchi, Theoretical basis of the Organic Rankine Cycle, Org. Rank. Cycle Power Syst. Technol. Appl., Elsevier Inc. (2017) 3–24, https://doi.org/10.1016/B978-0-08-100510-1.00001-6.
[32] S. Mucci, A. Bischi, S. Briola, A. Baccioli, Small-scale adiabatic compressed air energy storage: Control strategy analysis via dynamic modelling, Energy Convers. Manag. 243 (2021), 114358, https://doi.org/10.1016/j.enconman.2021.114358.
[33] A. Liponi, A. Baccioli, D.V. Candeas. Ferrari L. Seawater desalination through reverse osmosis driven by ocean thermal energy conversion plant: thermodynamic and economic feasibility. n.d.
[34] https://www.nist.gov/Reference Fluid Thermodynamic and Transport Properties Database (REFPROP) n.d. programs-projects/reference-fluid-thermodynamic-and-transport-properties-database-refprop (accessed May 18, 2023).
[35] A. Giwa, S.O. Giwa. Estimating the optimum operating parameters of olefin metathesis reactive distillation process 2013;8.
[36] H. Miton, Y. Doumandji, J. Chauvin, I De. Mecanique. Copyright © 1984 by ASME 2016:1–6.
[37] W. Sherwood. Renewable energy from the oceans: a guide to OTEC William H. Avery and Chih Wu, 1994, 446 pp. University Press. Ocean Eng 1995;22:763.
[38] R. Pili, N. Siamisiis, R. Agromayor, L.O. Nord, C. Wieland, H. Spliethoff. Efficiency Correlations for Off-Design Performance Prediction of ORC Axial-Flow Turbines. 5 Th Int Semin ORC Power Syst 2019.
[39] X. Fang, Q. Dai, Y. Yin, Y. Xu, A compact and accurate empirical model for turbine mass flow characteristics, Energy 35 (2010) 4819–4823, https://doi.org/10.1016/j.energy.2010.09.006.
[40] M. Deli, J. Fritz, S. Mateiescu, M. Busch, J.A. Carrino, J. Becker, et al., Hysys 2004, Cardiovasc. Interv. Radiol. 36 (2013) 748–755.
[41] L. Urbanucci, J.C. Bruno, D. Testi, Thermodynamic and economic analysis of the integration of high-temperature heat pumps in trigeneration systems, Appl. Energy 238 (2019) 516–533, https://doi.org/10.1016/j.apenergy.2019.01.115.
[42] E. Nebot, J.F. Casanueva, R. Solera, C. Pendòn, L.J. Taracido, T. Casanueva-Robles, C. Lòpez-Galindo. Marine Biofouling in Heat Exchangers 2010 Types, Impact and Anti-Fouling Biofouling. ISBN 978-1-60876-501-0.
[43] R. Turton, R. C. Bailie WBW e JAS. Analysis, Synthesis and Design of Chemical Processes. Pearson; 2009.
[44] Ships & Commercial Vessels For Sale | Horizon Ship Brokers n.d. https://horizonship.com/ (accessed January 31, 2023).
[45] P. Wang, Q. Li, C. Liu, R. Wang, Z. Luo, P. Zou, et al., Comparative analysis of system performance of thermally integrated pumped thermal energy storage systems based on organic flash cycle and organic Rankine cycle, Energy Convers. Manag. 273 (2022), 116416, https://doi.org/10.1016/j.enconman.2022.116416.